Solution Structure of PAFP-S: A New Knottin-Type Antifungal Peptide from the Seeds of *Phytolacca americana*[†,‡]

Guang-Hua Gao,[§] Wei Liu,[§] Ji-Xun Dai,[||] Jin-Feng Wang,[||] Zhong Hu,[⊥] Ying Zhang,[§] and Da-Cheng Wang*[,§]

Laboratory of Molecular Biophysics, National Laboratory of Macromolecules, Institute of Biophysics, Chinese Academy of Sciences, Beijing 100101, China, and Kunming Institute of Botany, Chinese Academy of Sciences, Kunming 650204, China

Received January 25, 2001; Revised Manuscript Received June 27, 2001

ABSTRACT: The three-dimensional solution structure of PAFP-S, an antifungal peptide extracted from the seeds of *Phytolacca americana*, was determined using ^{1}H NMR spectroscopy. This cationic peptide contains 38 amino acid residues. Its structure was determined from 302 distance restraints and 36 dihedral restraints derived from NOEs and coupling constants. The peptide has six cysteines involved in three disulfide bonds. The previously unassigned parings have now been determined from NMR data. The solution structure of PAFP-S is presented as a set of 20 structures using ab initio dynamic simulated annealing, with an average RMS deviation of 1.68 Å for the backbone heavy atoms and 2.19 Å for all heavy atoms, respectively. For the well-defined triple-stranded β-sheet involving residues 8−10, 23−27, and 32−36, the corresponding values were 0.39 and 1.25 Å. The global fold involves a cystine-knotted three-stranded antiparallel β-sheet (residues 8−10, 23−27, 32−36), a flexible loop (residues 14−19), and four β-reverse turns (residues 4−8, 11−14, 19−22, 28−32). This structure features all the characteristics of the knottin fold. It is the first structural model of an antifungal peptide that adopts a knottin-type structure. PAFP-S has an extended hydrophobic surface comprised of residues Tyr23, Phe25, Ile27, Tyr32, and Val34. The side chains of these residues are well-defined in the NMR structure. Several hydrophilic and positively charged residues (Arg9, Arg38, and Lys36) surround the hydrophobic surface, giving PAFP-S an amphiphilic character which would be the main structural basis of its biological function.

It is well-known that plants have evolved highly effective defense mechanisms to restrict the growth of microorganisms inside their tissues. A wide array of antimicrobial peptides or proteins, produced either in a constitutional or in an inducible manner, are believed to be involved in such mechanisms (see reviews in refs *1* and *2*). So far, many plant peptides or proteins with antimicrobial activities in vitro have been identified including chitinases (*3*), chitin binding proteins and hevein-like peptides (*4*−*6*), β-1,3-glucanase (*7*), thionins (*8*), permatins (*9*), PR-1-type proteins (*10*), lipid-transfer proteins (*11*), plant defensins (*12*), and knottin-like peptides (*13*). Among others, thionins, plant defensins, and hevein-like and knottin-like peptides are all small (29−54 amino acids), highly basic (pI > 10), and cysteine-rich peptides, but they are highly divergent in their sequences and exhibit quite different antimicrobial activities. The mode of action for these peptides is still much debated; therefore, it is essential to provide the three-dimensional structure of the respective antimicrobial peptides for understanding the molecular mechanisms. To date, a series of 3D structures for thionins (*14*−*16*), plant defensins (*17, 18*), and hevein-like peptides (*19, 20*) have been reported. Even though two highly homologous antifungal peptides, Mj-AMP1 and Mj-AMP2, from *Marbles jalapa L.* have shown a knottin-like cysteine motif (*13*) in their sequences, so far no three-dimensional structure of an antifungal peptide that adopts the knottin fold has been determined experimentally.

Recently we isolated and cloned a new antifungal peptide from the seeds of *Phytolacca americana* (Pokeweed), designated PAFP-S,[1] which consists of 38 amino acid residues with 3 disulfide bridges (*21*). PAFP-S exhibits a broad spectrum of antifungal activity. Besides the strong activities for certain saprophytic fungi, it also inhibits some plant pathogens such as *Fusarium oxysporum*, *Fusarium graminearum*, *Alternaria tenuis*, and *Pyricularia oryzae*. PAFP-S has no inhibitory activity toward *Escherichia coli*. The sequence analysis suggested that PAFP-S belongs to the knottin-type antimicrobial peptide (*21*). In the present paper, we report the three-dimensional solution structure of PAFP-S determined by 2D ^{1}H NMR. It is the first structural model of the knottin-like antimicrobial peptides. The functional implications of the structure will also be discussed.

[†] This work was supported by the National Natural Science Foundation of China (Grant 30070162) and the State Basic Research Program of China (G19990756).

[‡] The ensemble of 20 NMR models and NMR-derived restraints have been deposited under PDB accession code 1dkc. The ^{1}H chemical shifts for PAFP-S have been deposited in the BioMagResBank (http://www.bmrb.wisc.edu) under BMRB accession number 4615.

* Corresponding author. Phone: +86-10-64888547; Fax: +86-10-64871293; E-mail: dcwang@sun5.ibp.ac.cn.

[§] Laboratory of Molecular Biophysics, Institute of Biophysics, CAS.

[||] National Laboratory of Biomacromolecules, Institute of Biophysics, CAS.

[⊥] Kunming Institute of Botany, CAS.

[1] Abbreviations: PAFP-S, antifungal peptide from seeds of *Phytolacca americana* (Pokeweed antifungal peptide from seeds); COSY, correlated spectroscopy; DQF-COSY, double-quantum-filtered correlated spectroscopy; NMR, nuclear magnetic resonance; NOE, nuclear Overhauser effect; NOESY, nuclear Overhauser effect spectroscopy; TOCSY, total correlation spectroscopy; RMS, root-mean-square.

10.1021/bi010167k CCC: $20.00
Published on Web 08/23/2001

MATERIALS AND METHODS

NMR Sample Preparation. PAFP-S was isolated from the seeds of *Phytolacca americana* and sequenced as described previously (*21*). Peptide purity (>95%) was confirmed by SMART Mini-S chromatography and mass spectroscopy. The NMR samples were prepared by dissolving 8 mg of PAFP-S in 0.5 mL of solvent consisting of 0.2 mM DSS, pH (or pD) 3.5. For experiments in ^2H_2O, the sample was repeatedly dissolved in 99.8% ^2H_2O and lyophilized with the final sample dissolved in 99.996% ^2H_2O. For experiments in H_2O, the sample was dissolved in 90% H_2O/10% ^2H_2O.

NMR Spectroscopy. Proton NMR spectra were collected on a Bruker DMX 600 spectrometer at 300 or 310 K. The monomeric state of the peptide was checked by recording a 2D TOCSY spectrum at a PAFP-S concentration of either 1 or 4 mM. No significant frequency shift was observed between the two samples. COSY, DQF-COSY, E.COSY, TOCSY, and NOESY experiments were performed in the phase-sensitive mode with different spin-lock and mixing times. Typically, the 2D ^{1}H NMR experiments were recorded over a period of 20−40 h, acquiring 384 or 512 t1 increments, with 128 scans per increment and 4096 data points per scan. The spectra were acquired with a spectral width of 7183.908 Hz in the F1 and F2 dimensions. Data processing was performed on a SGI Onyx2 workstation using FELIX software version 97 (Biosym Technologies, San Diego, 1997). The original data were zero-filled to 1024 complex points in F1, and a sinebell-squared window function with a $\pi/2$ (0 for COSY) phase shift was applied prior to Fourier transformation. Baseline correction was performed in the F2 dimension using the standard FLATT macro of FELIX.

Structure Calculations. $^3J_{N\alpha}$ coupling constants were obtained from the DQF-COSY. The dihedral torsion angle ϕ was restrained to $-65 \pm 25°$ for $^3J_{N\alpha}$ less than 6 Hz and to $-120 \pm 30°$ for $^3J_{N\alpha}$ greater than 8 Hz. For residues without well-resolved coupling constants and dihedral restraints, ϕ was constrained between $-35°$ and $-175°$, which includes all sterically possible values for non-Gly residues. Stereospecific resonance assignments were determined for the H_β methylene protons of 12 residues using established methods (*22*). χ^1 angles were constrained to $60 \pm 30°$, $180 \pm 30°$, and $-60 \pm 30°$, respectively.

Distance restraints were obtained from the 2D NOESY spectra with a mixing time of 300 ms in H_2O or 250 ms in ^2H_2O. The build-up curves for PAFP-S (300 K, 1 mM, pH 3.5, 90% H_2O/10% D_2O) showed that the correlation remains linear until the mixing time reaches 300 ms, which indicated the appropriateness of the mixing time used in the experiment. In addition, conservative upper-bound distances of 2.7, 3.5, and 5.0 Å were used throughout the structure calculation to minimize the artifacts caused by spin diffusion. All NOEs were divided into three main classes, corresponding to the following criteria: strong NOEs, 1.8 Å $\leq d \leq$ 2.7 Å; medium NOEs, 1.8 Å $\leq d \leq$ 3.5 Å; and weak NOEs, 1.8 Å $\leq d \leq$ 5.0 Å. Pseudoatom corrections were applied to the upper limits of degenerate or unassigned methylene, methyl, or aromatic ring groups (*23*). In addition, 0.5 Å was added to all short- and medium-range restraints involving methyl groups.

Table 1: NOE Connectivities Defining Disulfide Pairings

disulfide bridge	interresidue NOE connectivity
Cys3−Cys20	HN Ile 4−HN Cys20
Cys10−Cys24	HA Cys10−HB1 Cys24
Cys19−Cys35	HB1 Cys19−HA Cys35
	HB2 Cys19−HA Cys35
	HA Cys19−HB1 Cys35
	HB1 Cys19−HB2 Cys35
	HB2 Cys19−HB1 Cys35

Structural calculations were performed with XPLOR version 3.851 using the simulated annealing protocol (*24*) in three stages. Initially, a fully extended starting structure was generated. In the first stage, 100 structures were generated for each interactive cycle during the assignment of ambiguous NOEs and for satisfying distance restraints for partial overlapping NOE cross-peaks. The starting structure was subjected to 18 000 steps of molecular dynamics at 1000 K, followed by 9000 cooling steps to 300 K. Finally, 1000 steps of Powell energy minimization were performed. At all times, the structure was subjected only to backbone torsion angles (ϕ) and direct NOE-based distance restraints. No disulfide or hydrogen bond restraints were applied. In the second stage, the structures were analyzed using the PROCHECK program (*25*) to determine more structural information: stereospecific assignments were obtained, and 12 slowly exchanging amide protons gave additional hydrogen bond restraints, namely, a 3.5 Å restraint between the amide nitrogen and carbonyl oxygen and a 2.5 Å restraint between the amide hydrogen and carbonyl oxygen. The new structural information was applied in the simulated annealing refinement. The disulfide bonds remained intact during this calculation. All 100 structures were passed through the refinement, which consisted of 12 000 cooling steps from 1500 to 100 K followed by 20 000 steps of Powell energy minimization. In the final stage of calculations, 20 structures were selected which had no NOE violations greater than 0.3 Å, had no dihedral angle violations larger than 3°, and had overall low energies as obtained from the XPLOR calculations.

RESULTS

Sequential Assignment and Disulfide Pairings. The complete sequence-specific assignment of the ^{1}H NMR resonance of PAFP-S was obtained using the standard methods established by Wüthrich and co-workers (*26*). The proton chemical shifts are presented as Supporting Information.

The three-dimensional structure of PAFP-S is stabilized by three disulfide bridges. In the absence of chemical characterization, these covalent links were determined from NMR data. The distance between the H_β protons of one Cys residue and the H_α proton of the second one engaged in the same disulfide bridge is in a range in which NOEs can be theoretically detected. Nevertheless, local dynamics or the mutual overlap between the H_β resonances of cystinyl and other residues can strongly hamper the detection of these NOEs. Several intercystinyl NOE connectivities allowed us to unambiguously identify two disulfide bridges: Cys10−Cys24 and Cys19−Cys35 (Table 1). The third bridge (Cys3−Cys20) was deduced indirectly via long-range connectivities between residues Cys20 and Ile4. The proposed disulfide pairings, Cys3−Cys20, Cys10−Cys24, and Cys19−Cys35,

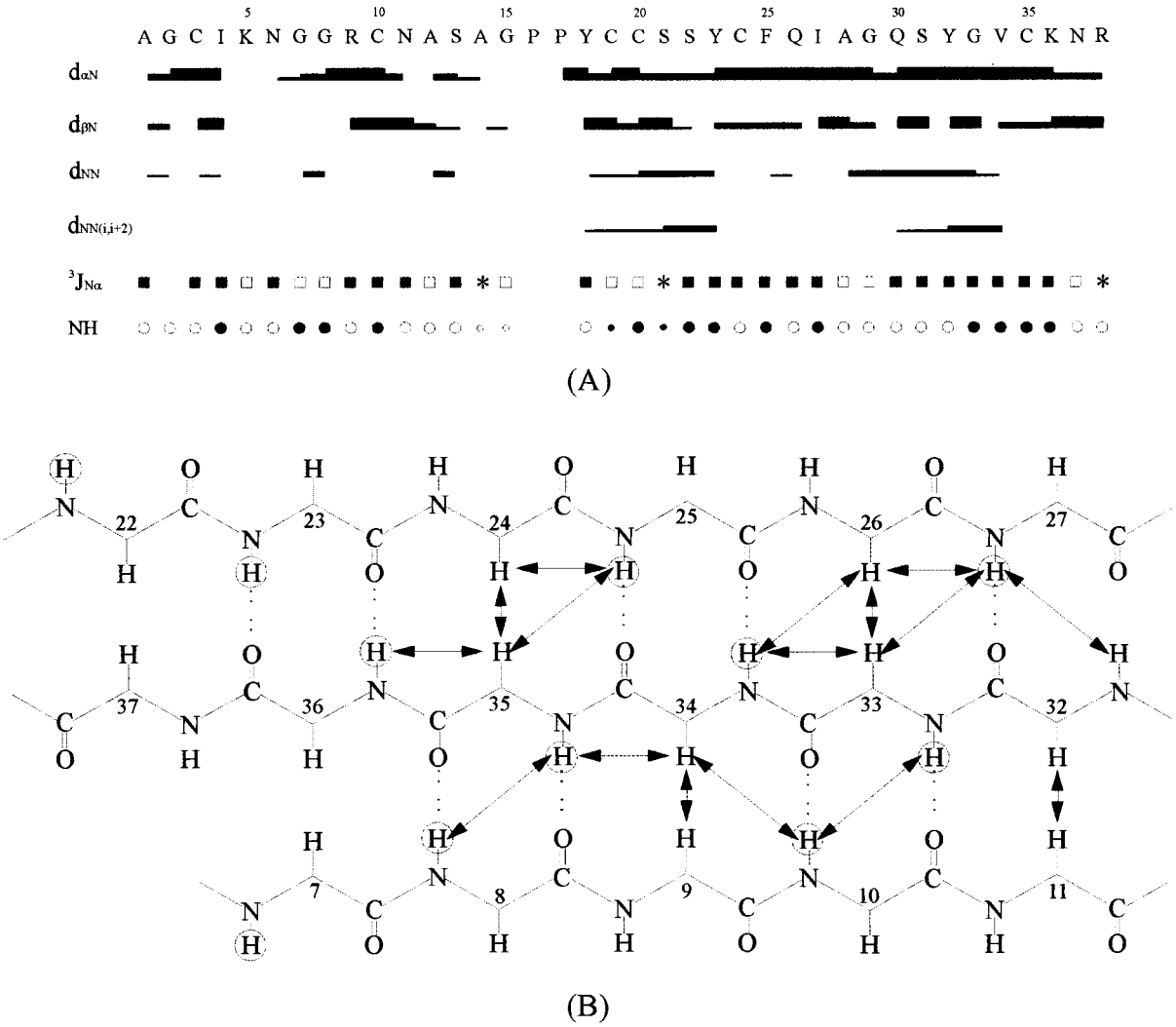

FIGURE 1: (A) Overview of the structural data for PAFP-S obtained from the NMR data. Sequential NOEs are categorized in distance ranges $d < 2.70$ Å (thick bars), 2.70 Å $\leq d \leq 3.50$ Å (thin bars), and $d > 3.50$ Å (lines). Amide H/^{2}H exchange rates (◯, fast; ○, <6 h; ●, >6 h; ●, >48 h) and coupling constants (□, $J < 6$ Hz; *, 6 Hz $\leq J \leq 8$ Hz; ■, >8 Hz). (B) Schematic representation of the antiparallel β-sheet structure of PAFP-S deduced from analysis of the NMR data. The observed interstrand NOE connectivities between backbone NH and CαH protons are indicated by arrows. The observed slowly exchanging amide protons (>48 h) are circled. The hydrogen bonds deduced from the NOE patterns and slowly exchanging amide protons are shown as dashed lines.

are fully compatible with the disulfide bond pattern found for a group of peptides collectively termed "knottins" (*27*).

Secondary Structure. The delineation of the regular secondary structure of PAFP-S from NMR data is based on the characteristic set of interstrand αH_i-NH_j, $NH_i-\alpha H_j$, and $\alpha H_i-\alpha H_j$ NOE contacts, $^3J_{N\alpha}$ coupling constants, slowly exchanging amide protons, and low-field-shifted H_α chemical shifts (*28*) as shown in Figure 1A. This is particularly evident from the interstrand αH_i-NH_j (Gln26−Val34), NH_i-NH_j (Gly8−Cys35, Cys10−Gly33, Ile27−Tyr32), and $NH_i-\alpha H_j$ (Cys10−Val34, Phe25−Cys35, Ile27−Gly33) NOE contacts as well as the well-characterized low-field-shifted H_α chemical shifts (relative to the random coil values) and large $^3J_{N\alpha}$ coupling constants. The antiparallel nature of the sheet is revealed by the typical interstrand αH_i-NH_j (Arg9−Val34, Asn11−Tyr32, Cys24−Cys35, Gln26−Gly33) NOEs (Figure 1B). As expected, most of the backbone amide protons within these strands exchange very slowly in D_2O while those lying outside individual β-strands exchange rapidly. The fast exchanging NH protons and the lack of NOEs suggest that several NH_2-terminal and COOH-terminal residues, and residues from Asn11 to Tyr18, are mobile and disordered in solution. So, we conclude that PAFP-S adopts a knot-like fold characterized by a compact three-stranded antiparallel β-sheet and a long loop connecting the first to the second β-strand (see Figures 2 and 3). This fairly rigid conformation, constrained by three disulfide bridges, ensures the excellent thermostability of PAFP-S.

The presence of several medium-range NOEs in the remainder of the structure suggests that it consists mainly of loops and turns. A total of 302 distance restraints [124 intraresidual, 86 sequential, 23 medium range ($|i - j| \leq 5$), and 69 long range] were extracted from the NOESY spectra. Their distribution over the sequence is shown as Supporting Information. Since there was no severe peak overlap and the dispersion of the proton resonances was fairly good, nearly 95% of peaks with reliable intensity were unambiguously assigned. The small number of NOEs used for the structure calculation is mainly due to the intrinsic flexibility of many residues in this peptide. Among 38 residues, 19 residues lack long-range NOE and most have less than 4 NOEs per residue. There is an average of 18 NOEs per residue, if these flexible residues are excluded (see Figure 2 in Supporting Information). NOE restraints, augmented by

Table 2: Structural Statistics of the 20 Best Structures of PAFP-S

mean rms deviations from exptl restraints	
distance (Å)	0.03418 ± 0.00171
dihedrals (deg)	0.2819 ± 0.12510
mean rms deviations from idealized geometry	
bond distances (Å)	0.00247 ± 0.00011
angles (deg)	0.55499 ± 0.01431
impropers (deg)	0.36785 ± 0.00666
pairwise atomic rms differences (Å)	
all residues	
backbone atoms	1.68 ± 0.48
all heavy atoms	2.19 ± 0.41
secondary structure	
backbone atoms	0.39 ± 0.11
all heavy atoms	1.25 ± 0.29

stereospecific assignments, torsion restraints, and hydrogen bond restraints, engender confidence in the quality of our structure.

Structural Statistics. The distribution in the Ramachandran plot of all residues (except the terminal residues and Pro) of the best 20 structures obtained by simulated annealing indicates the overall quality: 64.3% of the residues are in the most favored regions, 33.6% in additional allowed regions, and 2.1% in generously allowed regions. Table 2 lists the structural statistics for the set of structures. All structures are in excellent agreement with the experimental data and are fully compatible with the standard covalent geometry since the RMS deviation values from the ideal geometry are very low (Table 2).

Global Fold. The set of 20 structures representing the solution structure of PAFP-S is shown in Figure 2. It indicates the overall quality of the structure, and gives an impression of its main features. The RMS deviation values for backbone atoms and all heavy atoms are 1.68 and 2.19 Å, respectively (see Table 2). The main structural element in PAFP-S is an antiparallel β-sheet composed of three strands: Gly8−Cys10, Tyr23−Ile27, and Tyr32−Lys36 (Figure 3A). This part of the structure is well-defined, and pairwise RMS deviation values are very low (0.39 ± 0.11 Å for the backbone atoms and 1.25 ± 0.29 Å for all non-hydrogen heavy atoms). All hydrogen bonds expected to occur in the β-sheet are well represented over the 20 structures (100% persistent) and are all supported by the slow H/^{2}H exchange rates. Four β-reverse turns are found according to the notation of Efimov (*29*), including residues 4−8 ($\beta\alpha\gamma\alpha_L\beta$), 11−14 ($\beta\alpha\gamma\beta$), 19−22 ($\beta\alpha\gamma\beta$), and 28−32 ($\beta\alpha\gamma\alpha_L\beta$) (Figure 3A). The relative low backbone RMS deviation values of these turns indicate that their local conformation is well-defined, especially for turns 3 and 4. In contrast to the above structured regions, the N-terminal segment and a long loop from Ala14 to Cys19 are poorly defined, corresponding to the lack of long-range NOEs for these residues.

Amphipathic Surface. Many hydrophobic residues of PAFP-S are clustered on one side of the β-sheet, especially residues Tyr23, Phe25, Ile27, Tyr32, and Val34. Their side chains locate on the same side of β-strands S2 and S3, and they are well-defined in the NMR structure because a lot of the NOE cross-peaks are observed among them. These bulky hydrophobic residues rich in aromatic groups are close enough to each other to form a large hydrophobic surface on the exterior of the molecule (Figure 3B). Around this hydrophobic surface, there are several cationic sites formed by positively charged side chains including the most conservative residues Arg9, Lys36, and Arg38. These cationic sites are spatially adjacent to the hydrophobic residues. Together they constitute an amphipathic face (Figure 3). This is the most attractive structural feature of the PAFP-S molecule.

DISCUSSION

Structural Relationship with Other Proteins. Ten years ago, Le Nguyen et al. (*27*) first recognized a unique three-dimensional fold which featured a cysteine-knotted triple-stranded β-sheet. Based on this "knot-like" feature, they introduced the term "knottins" for this molecular scaffold. We now know that the knottins are a group of structurally related small proteins, typically less than 40 residues in length. Knottins bind to a diverse range of molecular targets to perform distinct functional activities but share a common scaffold comprising a small triple-stranded antiparallel β-sheet and disulfide bond framework with a consensus sequence (C···C···CC···C···C) and pairing pattern (1−4, 2−5, 3−6) (see Figure 4). To date, a series of knottins with high specificity to their target molecules, such as cellulose binding domain (*30, 31*), K^+ channel binding toxin (*32*), N- and P-type Ca^{2+} channel binding toxin (*33*), trypsin and α-amylase inhibitor (*34*), and sweet taste suppressing peptide (*35*), have been reported. However, no knottin structure that exhibits an antifungal activity has previously been reported.

Detailed inspection shows that the structure of PAFP-S described in this paper (see Figure 3) features all characteristics of the knottin fold. Thus, PAFP-S is a new member of the knottin protein group, which represents a novel binding specificity of the knottin fold. The knottin scaffold appears to be a promising architecture for the design of small proteins with diverse activities (*31, 35*). The structure of PAFP-S provides a new model of the mimetics.

In fact, the PAFP-S structure is the first antifungal peptide that adopts the knottin fold reported so far. Only two other antifungal peptides, Mj-AMP1 and Mj-AMP2, were reported to have the knottin-like cysteine motif. These two highly homologous peptides were purified from the seeds of *Mirabilis jalapa L.* and comprise 36 and 37 residues, respectively (*13, 37*). They also have 57% sequence homology to PAFP-S and share the same cysteine framework with PAFP-S (Figure 4). Thus, we predict that Mj-AMPs will adopt the knottin fold, similar to that of PAFP-S.

Structure−Activity Relationship. Compared with other plant antimicrobial peptides such as thionins and plant defensins, the knottin-like antimicrobial peptide has been investigated less intensively. The feature of the PAFP-S structure presented in this paper has given a certain insight into the structure−function relationship. As described above, the tertiary structure of PAFP-S has some obvious characteristics. First, all aromatic residues (Tyr23, Phe25, Tyr32), except Tyr18, are gathered onto one face of the molecule in close proximity to residues Ile27 and Val34 to form a hydrophobic surface (see Figure 3). Second, all three positively charged residues of the molecule, Arg9, Lys36, and Arg38, are also distributed on the same exterior surface that surrounds the above hydrophobic area to create a cationic hydrophilic zone. These two parts combine with each other to constitute an amphiphilic face on the PAFP-S exterior

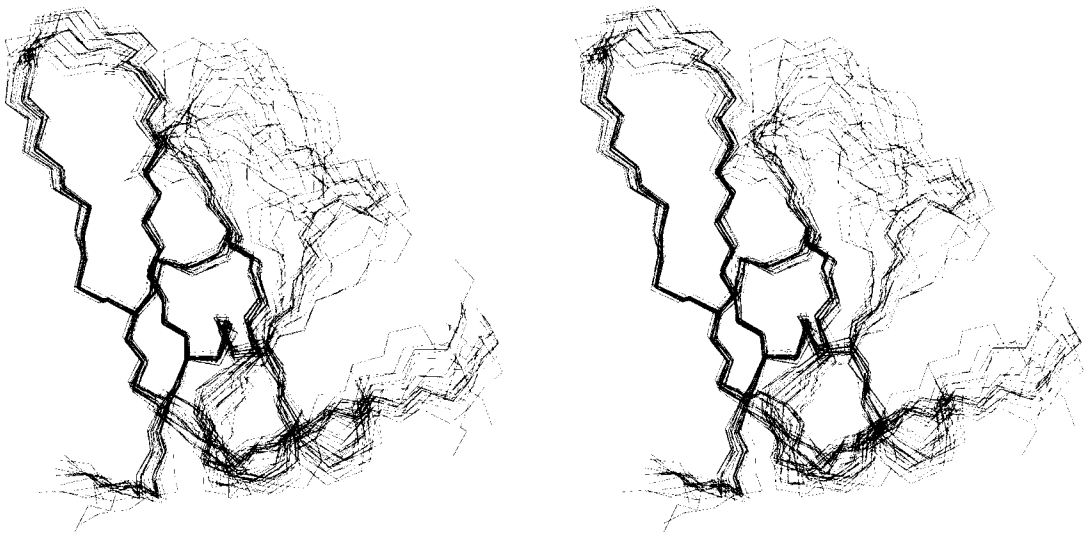

FIGURE 2: Ensemble of 20 structures of PAFP-S. The program MOLMOL was used to calculate a superposition of the backbone atoms of residues 8−10, 23−27, and 32−36.

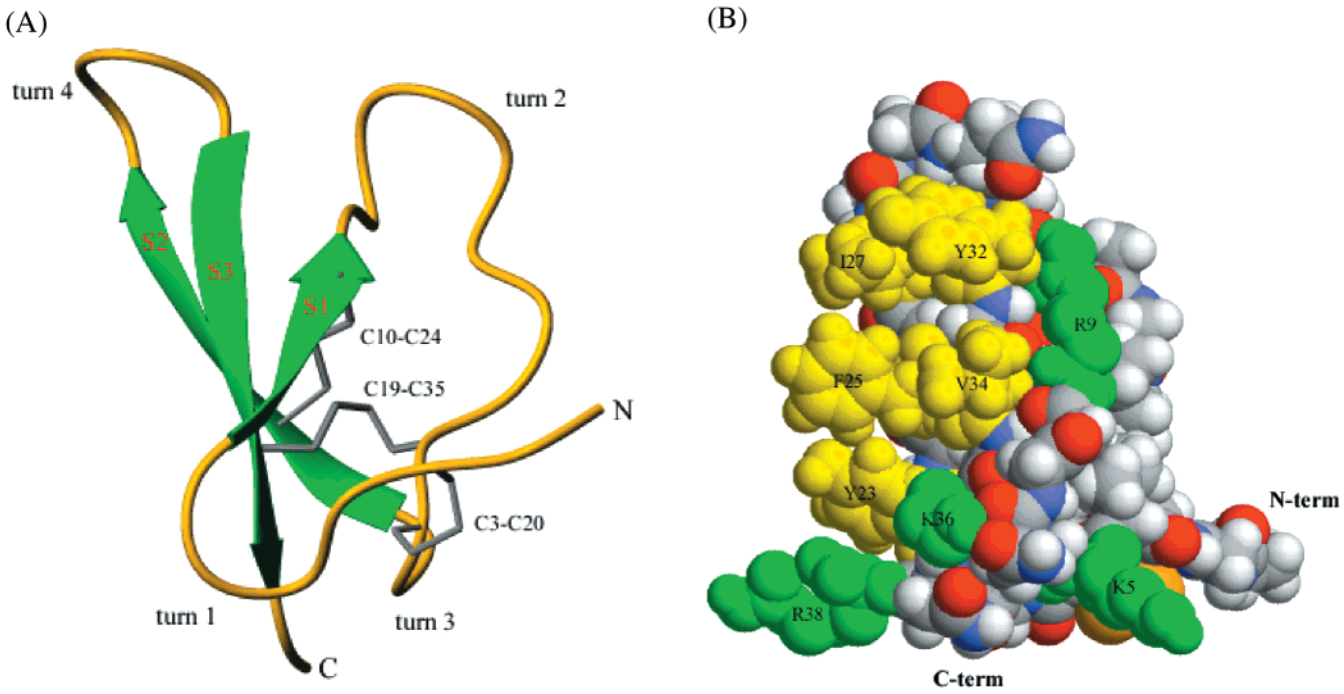

FIGURE 3: General structure of PAFP-S. (A) Ribbon plot of the backbone structure of PAFP-S. The representative model 1 is drawn with β-strands in green and disulfide bonds in gray. (B) Space-filling model of PAFP-S (representative model 1) showing an amphipathic face formed by a hydrophobic surface (yellow) and a hydrophilic zone (green) consisting of residues Tyr23, Phe25, Ile27, Tyr32, and Val34 as well as Arg9, Lys36, and Arg38, respectively, which may be involved in the action of PAFP-S with the target membrane.

(Figure 3B). The knottin-type peptide usually uses different faces of the molecular scaffold for interaction with different targets (*31, 38*−*40*). Based on the fact that all antimicrobial peptides studied so far have amphiphilic surfaces, which are well-suited for membrane binding (*41*), we hypothesize that this amphiphilic face is the main functional site of PAFP-S and it interacts with biomembranes.

The three charged residues of PAFP-S, Arg9, Lys36, and Arg38, are highly conserved among the knottin-type antifungal peptides (see Figure 4). In a bioassay for the antifungal peptide Mj-AMPs, the presence of Ca^{2+} and K^+ reduced the antifungal activity about 10 times (*13*). These data indicate that the charged residues may play an essential role in bioactivity of this kind of antifungal peptide. The sequence comparison (Figure 4) showed that the residues comprising the hydrophobic surface, i.e., Tyr23, Phe25, Ile27, Tyr32, and Val34, are variable between PAFP-S and Mj-AMPs. Considering that PAFP-S and Mj-AMPs exhibit distinct antifungal selectivity against different species of fungi (*21*),we hypothesize that the hydrophobic residues correlate with the specificity of PAFP-S to the fungal cell.

SUPPORTING INFORMATION AVAILABLE

Included are the proton chemical shifts in H_2O solution, a part of TOCSY and NOESY spectra, NOE distance restraints per residue, and the Ramachandran plot. This material is available free of charge via the Internet at http://pubs.acs.org.

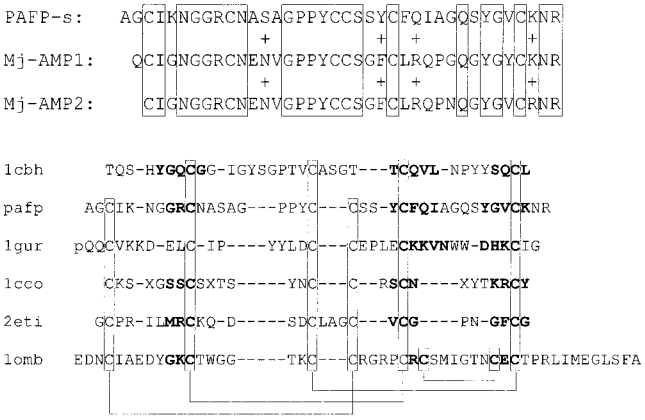

FIGURE 4: Sequence comparison of some knottin peptides. All sequences have been aligned by forcing the matching of cysteine residues which paired with the same pattern of 1−4, 2−5, and 3−6. The first three, PAFP-S (*21*), Mj-AMP1, and Mj-AMP2 (*13*), are antifungal peptides in which those residues identical to each other are boxed; others are as follows: 1cbh, the cellulose binding domain from *T. reset* (*30*); 1qur, the sweet taste suppressing peptide from the leaves of *Gymnema syevestre* (*35*); 1cco, the ω-conotoxin GVIA from the cone snit *Conus gengraphicus* (*33*); 2eti, the squash trypsin inhibitor EETI-II from the seeds of *Ecballium elarium* (*27*); lomb, the spider toxin OMEGA-AGA-IVB (*42*). Except for Mj-AMPs, all peptides listed here have their 3D structural model in which the residues involved in β-strands are marked with boldface characters.

REFERENCES

1. Broekaert, W. F., Cammue, B. P. A., De Bolle, M. F. C., Thevissen, K., De Samblanx, G. W., and Osborn, R. W. (1997) *Crit. Rev. Plant Sci. 16*, 297−323.
2. Fritig, B., Heitz, T., and Legrand, M. (1998) *Curr. Opin. Immunol. 10*, 16−22.
3. Collinge, D. B., Kragh, K. M., Mikkelson, J. P., Nielsen, K. K., Rasmussen, U., and Vad, K. (1993) *Plant J. 3*, 31−40.
4. De Boll, M. F. C., David, K. K. M., Rees, S. B., Vanderleyden, L., Cammue, B. P. A., and Broekaert, W. F. (1993) *Plant Mol. Biol. 22*, 1187−1190.
5. Van Parijs, J., Broekaert, W. F., Goldstein, I. J., and Peumans, W. J. (1991) *Planta 183*, 258−264.
6. Broekaert, W. F., Cammue, B. P. A., Osborn, R. W., and Rees, S. B. (1994) International Patent Application WO 94/115.
7. Manners, D. J., and Marshell, J. J. (1973) *Phytochemistry 12*, 547−553.
8. Bohlman, H., and Apel, K. (1991) *Annu. Rev. Plant Physiol. Plant Mol. Biol. 42*, 227−240.
9. Vigers, A. J., Roberts, W. F., and Selitrennikoff, C. P. (1991) *Mol. Plant−Microbe Interact. 4*, 315−323.
10. Niderman, T., Genetet, I., Brugere, T., Gees, R., Stintzi, A., Legrand, M., Fritig, B., and Mosinger, E. (1995) *Plant Physiol.* (Bethesda) *108*, 17−27.
11. Cammue, B. P. A., Thevissen, K., Hendriks, M., Eggermont, K., Goderis, I. J., Proost, P., Van Damme, J., Osborn, R. W., Guerbette, F., Kader, J. C., and Broekaert, W. F. (1995) *Plant Physiol. 109*, 445−455.
12. Terras, F. R. G., Eggermont, K., Kovaleva, V., Raikhel, N. V., Osborn, R. W., Kester, A., Rees, S. B., Torrekens, S., Vanleuven, F., Vanderleyden, J., Cammue, B. P. A., and Broekaert, W. F. (1995) *Plant Cell 7*, 571−588.
13. Cammue, B. P. A., De Bolle, M. F. C., Terras, F. R. G., Proost, P., Van Damme, J., Rees, S. B., Vanderleyden, J., and Broekaert, W. F. (1992) *J. Biol. Chem. 267*, 2228−2233.
14. Hendrickson, W. A., and Teeter, A. M. (1981) *Nature 290*, 107−113.
15. Clore, G. M., Nilges, M., Sukumaran, D. K., Brienger, A. T., Karplus, M., and Gronenborn, A. M. (1986) *EMBO J. 5*, 2729−2735.
16. Stec, B., Rao, V., and Teeter, M. M. (1995) *Acta Crystallogr., Sect. D 51*, 914−924.
17. Bnux, M., Jimenez, M. A., Santora, J., Gonzalez, C., Collilla, F. J., Mendez, E., and Rico, M. (1993) *Biochemistry 32*, 715−724.
18. Fant, F., Franken, W. F., Martins, J. C., and Borremans, F. A. M. (1996) *Bull. Soc. Chim. Belg. 106*, 51−57.
19. Andersen, N. H., Cao, B., Rodriguez-Romero, A., and Arreguin, B. (1993) *Biochemistry 32*, 1407−1422.
20. Martins, J. C., Maes, D., Loris, R., Pepermans, H. A. M., Wyns, L., Willem, R., and Verheyden, P. (1996) *J. Mol. Biol. 258*, 322−333.
21. Shao, F., Hu, Z., Xiong, Y. M., Huang, Q. Z., Wang, C. G., Zhu, R. H., and Wang, D. C. (1999) *Biochim. Biophys. Acta 1430*, 262−268.
22. Hyberts, S. G., Märki, W., and Wagner, G. (1987) *Eur. J. Biochem. 164*, 625−635.
23. Wüthrich, K., Billeter, M., and Braun, W. (1983) *J. Mol. Biol. 169*, 949−961.
24. Brunger, A. T. (1992) *X-POLR (Version 3.1) Manual*, Yale University Press, New Haven, CT.
25. Laskowski, R. A., MacArthur, M. W., Moss, D. S., and Thornton, J. M. (1993) *J. Appl. Crystallogr. 26*, 283−291.
26. Wüthrich, K. (1986) *NMR of Proteins and Nucleic Acids*, John Wiley and Sons, New York.
27. Le Nguyen, D., Heitz, A., Chiche, L., Gastro, B., Boigegrain, R. A., Favel, A., and Coletti-Previero, M. A. (1990) *Biochimie 72*, 431−435.
28. Wishart, D. S., Sykes, B. D., and Richards, F. M. (1992) *Biochemistry 31*, 1647−1651.
29. Efimov, A. V. (1993) *Prog. Biophys. Mol. Biol. 60*, 201−239.
30. Kraulis, P. J., Clore, G. M., Nilges, M., Jones, T. A., Pettersson, G., Knowles, J., and Gronenborn, A. M. (1989) *Biochemistry 28*, 7241−7257.
31. Smith, G. P., Patel, S. U., Windass, J. D., Thornton, J. M., Winter, G., and Griffiths, A. D. (1998) *J. Mol. Biol. 277*, 317−332.
32. Bontems, F., Roumestand, C., Gilquin, B., Menez, A., and Toma, F. (1991) *Science 254*, 1521−1523.
33. Narasihman, L., Singh, J., Humblet, C., Guraprasad, K., and Blundell, T. (1994) *Nat. Struct. Biol. 1*, 850−852.
34. Chagolla-Lopez, A., Blanco-Labra, A., Patthy, A., Sanchez, R., and Pongor, S. (1994) *J. Biol. Chem. 269*, 23675−23680.
35. Arai, K., Ishima, R., Morikawa, S., Miyasaka, A., Imoto, T., Yoshimura, S., Aimoto, S., and Akasaka, K. (1995) *J. Biomol. NMR 5*, 297−305.
36. Vita, C. (1991) *Curr. Opin. Biotechnol. 8*, 429−434.
37. De Boll, M. F. C., David, K. K. M., Rees, S. B., Vanderleyden, L., Cammue, B. P. A., and Broekaert, W. F. (1993) *Plant Mol. Biol. 22*, 1187−1190.
38. Lampe, R. A., Lo, M. M. S., Keith, R. A., Horn, M. B., McLane, M. W., Herman, J. L., and Spreen, R. C. (1993) *Biochemistry 32*, 3255−3260.
39. Sato, K., Park, N. G., Kohno, T., Maeda, T., Kim, J. I., Kato, R., and Takahashi, M. (1993) *Biochem. Biophys. Res. Commun. 194*, 1292−1296.
40. Kim, J. I., Takahashi, M., Ogura, A., Kohno, T., Kudo, Y., and Sato, K. (1994) *J. Biol. Chem. 269*, 23876−23878.
41. Hwang, P. M., and Vogel, H. J. (1998) *Biochem. Cell Biol. 76*, 235−246.
42. Yu, H., Rosen, M. K., Saccomano, N. A., Phillips, D., Volkmann, R. A., and Schreiber, S. L. (1993) *Biochemistry 32*, 13123−13129.

BI010167K